Article

Comprehensive Reservoir Architecture Dissection and Microfacies Analysis of the Chang 8 Oil Group in the Luo 1 Well Area, Jiyuan Oilfield

Jing Wang, Lixin Wang *, Yanshu Yin, Pengfei Xie and Ge Xiong

Key Laboratory of Exploration Technologies for Oil and Gas Resources, Ministry of Education, Yangtze University, Wuhan 430100, China; 2022710395@yangtzeu.edu.cn (J.W.); yys@yangtzeu.edu.cn (Y.Y.); pengfei.xie@yangtzeu.edu.cn (P.X.); 2023730052@yangtzeu.edu.cn (G.X.)
* Correspondence: wlx@yangtzeu.edu.cn; Tel.: +86-150-7119-9323

Abstract: The Chang 8 oil group within the Luo 1 well area of Jiyuan Oilfield, situated in the Ordos Basin, exemplifies an ultra-low-permeability reservoir with an average permeability of 0.84 mD. Despite primary development efforts through acid fracturing, suboptimal recovery efficiency has been observed due to inadequate injection–production matching. To mitigate this issue and enhance reservoir utilization, a comprehensive understanding of sand body architecture is imperative. This study employs a detailed reservoir architecture element analysis approach, integrating core samples, thin-section petrography, and geophysical logging data. The objective is to elucidate the internal structure and heterogeneity of sand bodies, which significantly influence hydrocarbon recovery. Key findings reveal that the study area is characterized by a shallow-water deltaic depositional system, featuring three principal sedimentary microfacies: subaqueous distributary channels, sheet sands, and lacustrine muds. Notably, subaqueous distributary channel sand bodies dominate, forming composite units via lateral accretion or vertical stacking of 2–5 individual channels, with widths exceeding 2000 m. Individual distributary channels range from 83 to 535 m in width, exhibiting both isolated and stacked contact styles. Importantly, only 25.97% of channels demonstrate connectivity, underscoring the critical role of channel scale and continuity in ultra-low-permeability reservoir development. By addressing the previously identified gap in architectural configuration knowledge, this study contributes foundational data for future development improvements. In conclusion, the detailed characterization of reservoir architecture offers pivotal insights into tailoring development strategies that align with the specific characteristics of ultra-low-permeability reservoirs, thereby improving overall recovery rates.

Keywords: ultra-low-permeability reservoir; shallow-water delta front; sand body architecture analysis; sedimentary microfacies; Ordos Basin

1. Introduction

The concept of shallow-water deltas was first proposed by Fisk during his study of the Mississippi River Delta [1], and was further enriched by Donaldson in his research on the Carboniferous terrestrial seas in the United States [2]. The sedimentary evolution and main controlling factors of Nenjiang Formation in North Da 'an area of the southern Songliao Basin are discussed, and two sedimentary models of shallow-water deltas are established [3]. Geer Zhao et al.'s study is predominantly intended to explore the distribution rule of the sand body of the Zhuhai Formation on the north slope of the Baiyun

Sag [4]. Channel dimensions are generally smaller in the medial areas, but sizes are variable: deposits are of braided, meandering, and simple channels which show varying degrees of lateral migration [5]. Sedimentological facies models for (semi-)isolated basins are less well developed than those for marine environments, but are critical for our understanding of both present-day and ancient deltaic sediment records in restricted depositional environments [6]. Currently, shallow-water delta sediments have been found in the Mesozoic and Cenozoic strata of basins such as Bohai Bay, Ordos, and Songliao in China [7]. These deposits have formed large-scale oil and gas reservoirs, showcasing significant exploration potential [8]. The delta-front sand bodies of shallow-water deltas are diverse in type, possess good reservoir properties, and offer favorable conditions for oil and gas accumulation, making them important reservoir facies for hydrocarbons. Therefore, conducting in-depth research on the delta-front architecture models of shallow-water deltas is crucial for future oil and gas exploration and development.

The Ordos Basin, a crucial Chinese oil and gas source, features low-permeability lithological reservoirs. These reservoirs have tight rock formations with minimal pore space, restricting fluid flow. During the Triassic period, the Chang 8 oil reservoir group of the Upper Triassic Yanchang Formation in the Ordos Basin experienced continuous subsidence and stable settling, forming shallow-water river–lake facies deposits with a river–lake source clastic rock sequence [9–11]. Among them, the Chang 8 oil reservoir group developed typical shallow-water delta deposits. Previous studies on the shallow-water delta depositional facies of the Yanchang Formation in the Ordos Basin have been extensive. Wang Changyong et al. [12], guided by high-resolution sequence stratigraphy analysis, conducted detailed stratigraphic correlations and small-scale sand body divisions for the Chang 8 oil group in the Jiyuan area. Based on this, they created a top structure map and a planar distribution map of the small sand bodies under isochronous conditions, which refer to the geological principle that all points on a given stratigraphic surface are of the same age. Li Yuanhao et al. [13], through extensive core observations, concluded that the Chang 8 oil reservoir group in the northwest part of the Ordos Basin predominantly developed shallow-water delta-front subfacies deposits. Subaqueous distributary channels were the main depositional microfacies, with large, far-reaching sand bodies characterized by local thick sand bodies in the river channel direction forming mound-like distributions, and mound-like sand bodies surrounding the lake basin in a ring-shaped pattern in the vertical river channel direction. Although there has been considerable research on the depositional microfacies and sedimentary characteristics of shallow-water deltas in the Ordos Basin, especially the Chang 8 oil reservoir group of the Yanchang Formation, studies on the characterization of individual sand bodies, especially in the context of their sedimentary background, remain relatively limited.

This article takes the Chang 8 oil reservoir group in the Luo 1 well area of the Jiyuan Oilfield as an example, utilizing core, logging, and production dynamic data to characterize individual sand bodies. It analyzes the distribution patterns of river channels and the stacking styles of various architecture units in the context of shallow-water delta-front subfacies. The accuracy of the architecture interpretation is verified through production dynamics, providing a basis for enhanced oil recovery, well pattern adjustments, and water injection development in the oilfield [14]. Prior research on this block has been limited in its exploration of architectural configuration, leaving a notable gap in the existing literature. The present study aims to rectify this omission by providing an in-depth analysis of the reservoir's structural characteristics, thereby contributing to a more comprehensive understanding of the geological setting.

2. Geological Setting

The Ordos Basin is a basin formed on an ancient and relatively stable continental plate, which has undergone multiple geological cycles and features layered structural overlays due to prolonged tectonic movements, sedimentation, and possible erosion. It is composed of six secondary structural units: the Yimeng Uplift, the Weibei Uplift, the Jinxi Nappe Belt, the Yishan Slope, the Tianhuan Depression, and the western erosion belt [15–17]. The basin has a simple structure with gently sloping strata, and the main feature is the Yishan Slope, which tilts westward at an angle of less than 1° [18]. The Middle to Upper Triassic Yanchang Formation deposition period is a critical sedimentary phase in the basin, forming 800–1200 m of inland river–lake facies strata, which are the main targets for oil and gas exploration in this area [19]. The Yanchang Formation is divided into 10 oil reservoir groups from top to bottom. After the deposition of the Chang 9 oil reservoir group, the Chang 8 oil reservoir group formed with mainly delta-front subfacies sediments [20–22].

The Luo 1 well area is located in the eastern part of the Tianhuan Depression in the Ordos Basin, neighboring the Shaanxi North Slope (Figure 1). It is an important oil-producing block of the Jiyuan Oilfield. Structurally, the area is characterized by a monocline that slopes from east to west, with no significant faulting or folding within the region. The oil-bearing area spans 33.9 km^2 and is considered a delta-front subfacies, with underwater distributary channel sedimentary microfacies forming the framework sandstone, which is a favorable oil and gas accumulation zone. Due to diagenesis, the permeability is extremely low, making it a typical ultra-low-permeability reservoir with poor reservoir properties and strong heterogeneity. In terms of development, acid fracturing is the primary engineering method used for such reservoirs [23]. However, there has been limited research on the internal structure and interfaces of the reservoir itself, leading to poor correspondence between injection and production during extraction and low production efficiency. The sand body architecture directly influences the development results. Therefore, it is urgently needed to conduct a detailed characterization of the internal architecture of single sand bodies, identify how different architectural styles impact the oil–water connectivity of well groups, and reveal the oil–water flow patterns to provide a reference for the future recovery of remaining oil [24]. To enhance the explanation of oil–water flow patterns for more effective recovery of residual oil, it is imperative to integrate sophisticated simulation models with empirical field data. A thorough analysis of fluid dynamics, reservoir pressure, and saturation levels should inform the optimization of well placement and the application of enhanced oil recovery techniques. Continuous monitoring and adaptive strategies, guided by real-time data, are crucial for maximizing extraction efficiency.
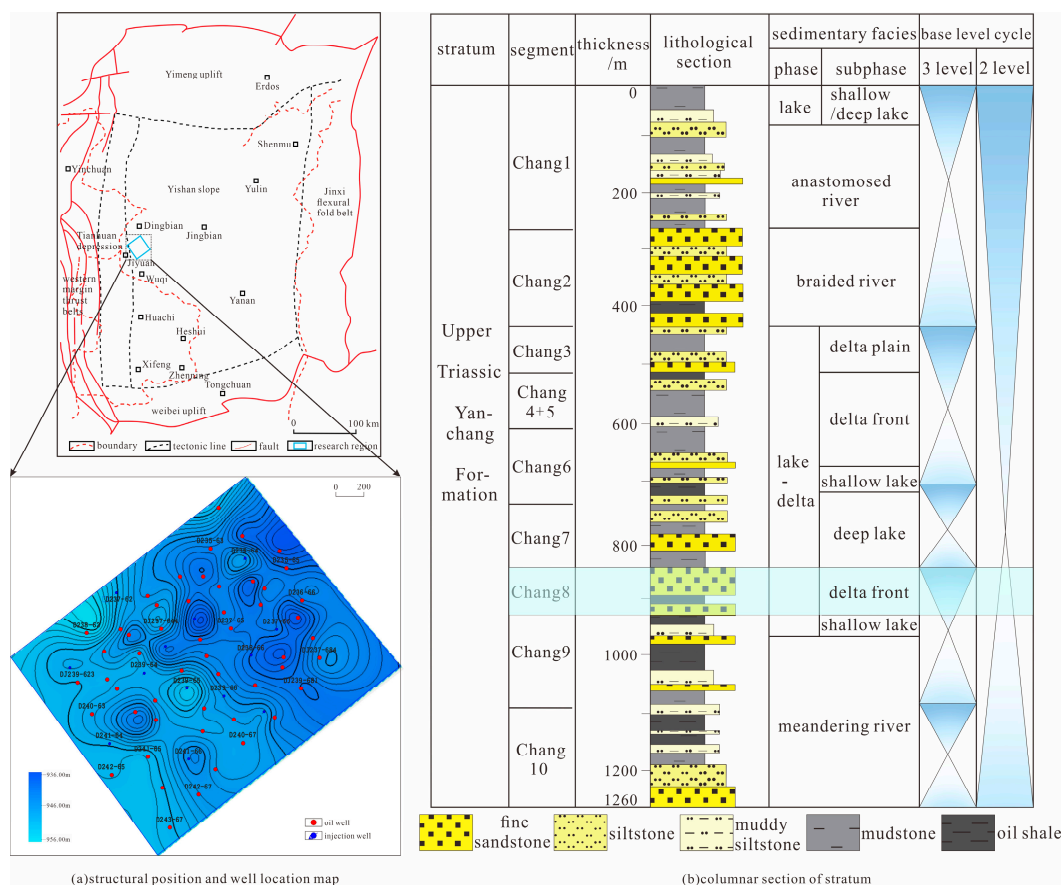
Figure 1. Tectonic setting and comprehensive stratigraphic column of the study area.

3. Materials and Methods

In this part of the study, data were obtained in August 2023 from the Changqing Oilfield E&P Research Institute in Xi'an, China, and the study was completed in December 2023.

3.1. Sedimentary Facies Characteristics

3.1.1. Sedimentary Microfacies Types

Core descriptions from two drilling wells in the study area indicate that the lithology of the Chang 8 section is predominantly composed of gray, light gray, and gray-brown fine sandstone (59.58%), gray and light gray mudstone siltstone (12.82%), dark gray silty mudstone (9.05%), and gray-black or dark gray mudstone (18.55%). In the siltstone and mudstone, occasional plant stem and leaf imprints are observed, reflecting that the sediment was not transported over long distances or underwent significant alteration. The clastic composition is primarily quartz, followed by feldspar. The relatively high content of feldspar and rock fragments indicates a lower compositional maturity of the sandstone, suggesting that the sandstones in this area were largely deposited near the source area. The mudstone is gray-black or dark gray, indicating a reducing underwater depositional environment [25–27].

Based on the analysis of thin section identification data of clastic rocks, the average maximum particle size is 0.58 mm. The particle sorting is good to medium, and the roundness is sub-angular. The cementation types include pore cementation, enhanced pore cementation, and film cementation. The pore types are mainly dissolution pores and intergranular pores, with a small portion being intergranular pores. The clastic particles are well sorted but poorly rounded, indicating moderate to low structural maturity. This

reflects that the sediments in the study area have undergone minimal transportation and depositional processes. The logging curves are predominantly box-shaped and bell-shaped, with some funnel-shaped curves (Figure 2).
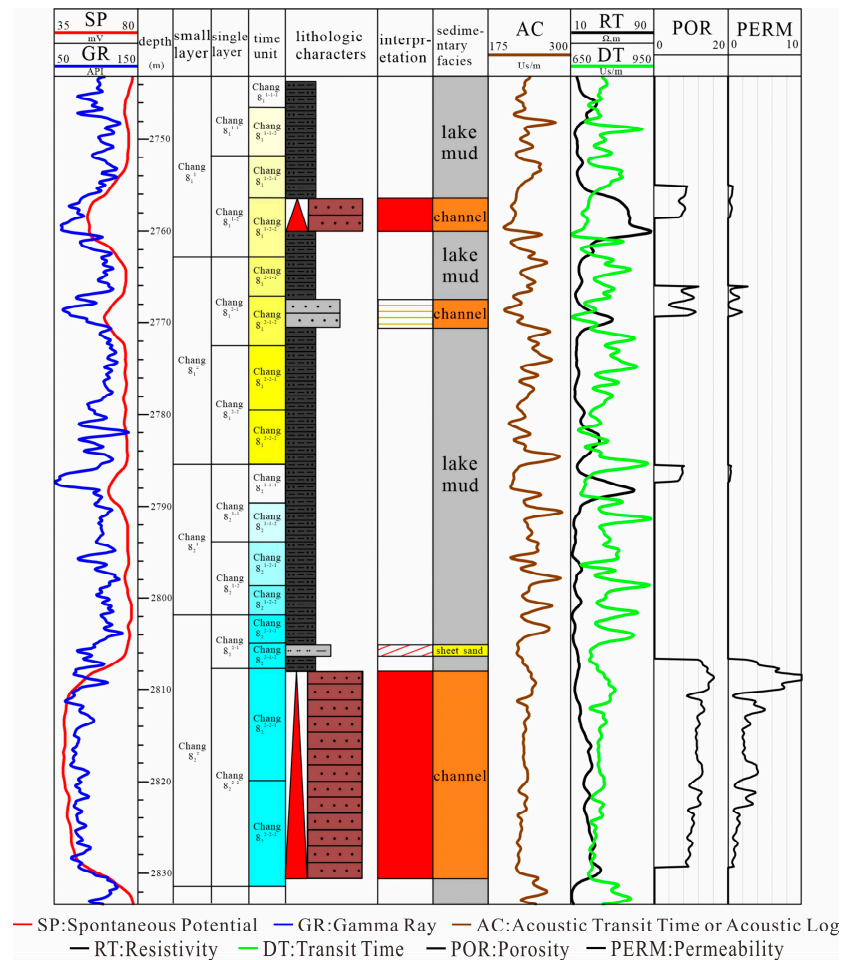

Figure 2. Core composite column diagram of well D237-67.

Based on core descriptions and log curve characteristics, the delta-front sandstone bodies in the study area are classified into three sedimentary microfacies types: subaqueous distributary channel, sheet sands, and lake mud.

Subaqueous distributary channels are extensions of river systems into the lakebed after rivers enter the lake, formed by the superposition of distributary channels from different stages. These channels create the framework for the small-scale reservoir layers and represent the area of high hydrodynamic deposition in the study region. The lithology is mainly gray and gray-brown fine sandstone, with a low clay content. The grain size follows a normal or composite rhythm. From the electrical logging curves, most of them show box-shaped or bell-shaped GR curve characteristics, with some exhibiting funnel–box shapes, reflecting multi-stage accumulation. The SP curve typically exhibits box-shaped or bell-shaped characteristics, with large negative anomalies, defined as significant deviations below the baseline, often exceeding several tens of millivolts in amplitude. The thickness of the multi-stage superposed channels is large, usually exceeding 8 m, and their width often exceeds 300 m. Single-stage channels generally show a bell-shaped curve, with a width not exceeding 300 m [28].

Sheet sands refer to thin sand layers and are a collective term for sheet sands and bar fingers. They are distributed from the delta front to the pre-delta region, with a stable sand body distribution and a relatively wide coverage area. The lithology is mainly gray

and light gray mud-bearing siltstone, with a finer grain size compared to the subaqueous distributary channel. The sand body thickness generally does not exceed 3 m, and the width is relatively narrow, generally not exceeding 100 m. Vertically, the sediment shows an anastomosing or poorly rhythmic pattern, with GR logging curves displaying funnel-shaped or finger-like profiles with thin layers and moderate amplitude. SP curves generally show funnel-shaped or finger-like profiles [29].

The lake mud microfacies refers to the sedimentary environment formed at the confluence of river tributaries, where changes in flow velocity and direction lead to varying deposition of materials, resulting in distinct microfacies features. The lithology is primarily grayish-black and dark gray silty mudstone or mudstone, with well-developed parallel lamination, and contains plant fossils, charcoal fragments, and other materials, exhibiting a blocky form. The rhythm is not well defined. The GR curve shows a high and relatively flat profile, while the SP curve shifts towards the baseline [30].

3.1.2. Planar Facies Distribution

Based on the logging facies markers of the three different microfacies mentioned above, a microfacies planar distribution prediction was conducted. The results show that the contiguous sand bodies in the study area are primarily distributed in the Chang 8_2^{2-2} layer, covering almost the entire work area with a width exceeding 2000 m. Additionally, the sheet sand bodies are located near the underwater distributary channel sand bodies.

From the planar map and the sand body isopach map (Figure 3), it can be observed that the sand body thickness across the entire well area is relatively thick, showing a full-basin sand distribution. The river channel and sheet sand depositional microfacies are well developed, with the river channels forming a continuous distribution [31]. The overall flow direction is from the northeast to the southwest. The thick sand bodies are mainly distributed in the northwest and southeast directions of the study area, while the sheet sand depositional microfacies are less developed in comparison to the Chang 8_2^{2-2-1} layer [32].

(a) the sand body isopach map in the Chang 8_2^{2-2-1} layer   (b) the planar map in the Chang 8_2^{2-2-1} layer
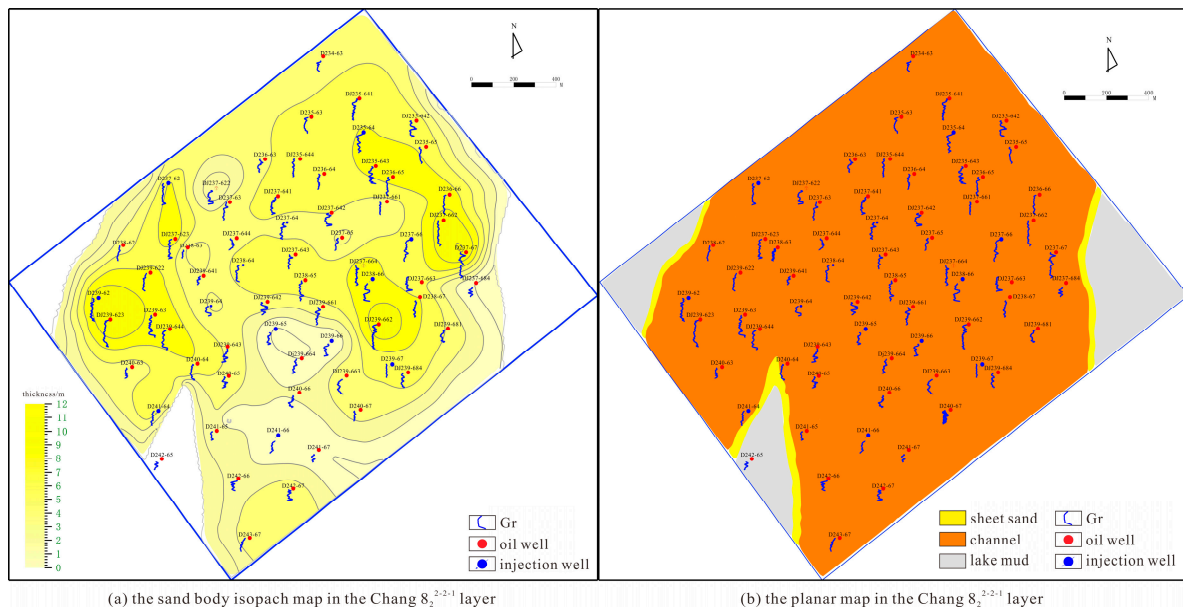
Figure 3. Sand body thickness map and depositional facies planar map of the Chang 8_2^{2-2-1} layer.

From the planar distribution of facies, it can be observed that the channel sand bodies from different periods are stacked on top of each other, and the sand bodies from the same period are cut off from each other, forming widespread contiguous sand bodies. This overlap masks the interfaces between sand bodies and their flow characteristics. Additionally,

different areas may develop intercalated layers, leading to mismatches between injection and production. Therefore, a detailed internal structural analysis of the contiguous sand bodies in the study area is necessary.

3.2. Delta-Front Reservoir Architecture Analysis

3.2.1. Composite Sand Body Architecture Analysis

Many methods have been proposed by previous researchers to analyze the subaqueous distributary channel of the delta front. For example, Ma et al. [33] took the Gaoshan 76 fault block of the Nanbao Depression as a case study to analyze the single sand body architecture characteristics in a fault-block small lake basin fan delta front. They summarized four lateral stacking patterns of single sand bodies and the "river flows over the levee" model. Yin et al. [34] focused on the Chang $6_1{}^1$ layer of the Sai 160 well area in the Anse Oilfield, where they identified the area as a typical meandering river shallow-water delta deposit. The sedimentary microfacies developed in the area included subaqueous distributary channels, delta-front bars, sheet sands, and bay deposits, with the channel deposits being the dominant sedimentary facies, showing a continuous distribution pattern. Yang et al. [8] combined core, well log, and seismic data to perform an architecture analysis of the lower section of the Minghuazhen Formation in the BZ25 Oilfield in Bohai. They explored the sedimentary microfacies composition inside the subaqueous distributary channel and analyzed the macroscopic distribution and internal architecture characteristics of the deltaic bar finger.

This study, based on the fine anatomy of the single-channel sand body in the target layer of the research area, summarizes five key boundary identification indicators of single sand bodies: sedimentary facies transitions, top elevation differences, thickness variations, curve morphology differences, and differences in oil and gas potential.

(1) Due to differences in depositional topography, the same sand body may bifurcate, resulting in the development of sheet sands or mudstone bands in the middle. Therefore, the presence of mudstone bands or sheet sands often indicates the boundaries of river channels. For instance, sheet sands are observed between wells D236-65 and D237-66, while mudstone appears between wells D237-66 and D238-67 (Figure 4a). Hence, it can be concluded that these represent different river channels.

(2) From the elevation difference marker, the top elevation of a single sand body should be consistent, as the sand bodies formed by different subaqueous distributary channels may have differences in elevation due to variations in the depositional paleotopography and developmental periods. If sand bodies are observed at different elevations on a profile, they can be interpreted as deposits from different subaqueous distributary channels. For example, although the sand bodies encountered in wells D241-64 and D240-65 are located in the same single sand layer, their top elevations are inconsistent (Figure 4b), indicating that they belong to different subaqueous distributary channels.

(3) The thickness of a single distributary channel sand body decreases from the center towards both sides. If there are differences or abrupt changes in the thickness variations between sand bodies, it is considered that the deposits are not from the same period. For example, wells D239-63, DJ239-641, and DJ237-644 exhibit a trend of thick–thin–thick (Figure 4c), indicating that a boundary between distinct distributary channels exists between them.

(4) In terms of logging curve responses, distributary channels from the same depositional period, due to similar material composition and subsequent modifications, show similar logging responses without significant abrupt changes. Moreover, sudden changes in curve amplitude or degree of "spikiness" could indicate the presence of boundaries. For instance, the logging curve for well D240-64 is box-shaped, while

the logging curve for well DJ239-643 is bell-shaped, showing a noticeable difference (Figure 4d), which indicates a boundary between the two wells.

(5) Generally speaking, underwater distributary channel sands from the same depositional period, after excluding structural differences, should exhibit similar oil and gas contents. During development, the water flooding characteristics of these sands should also be comparable. If two nearby wells show significant differences in oil and gas content in the same sand body, they can be considered to belong to different depositional periods. For instance, wells DJ237-641 and DJ235-644 encountered water-flooded sands in this layer, while well DJ235-641 interpreted the same layer as an oil-bearing zone (Figure 4e). This indicates the presence of a boundary between the two distributary channels.
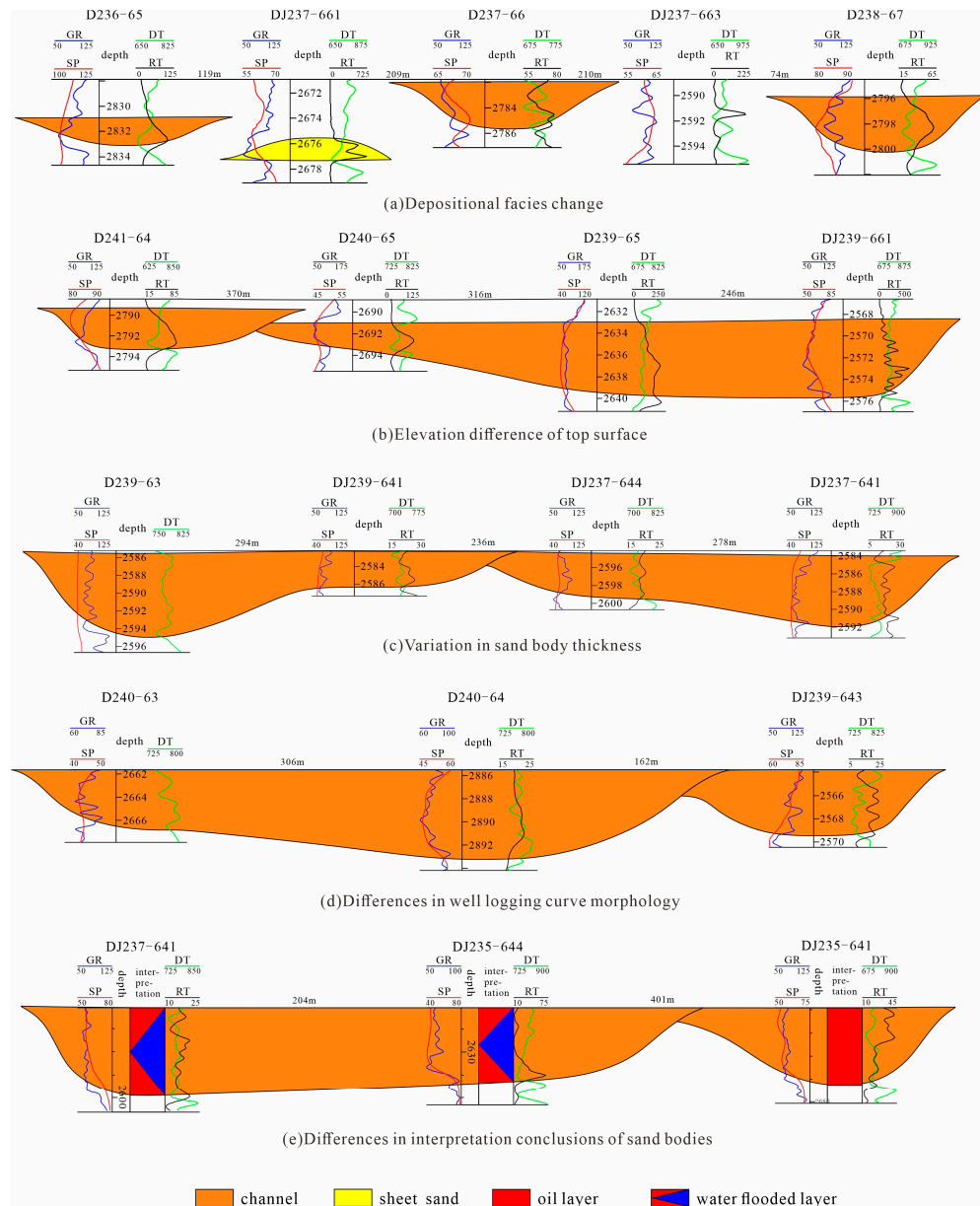

Figure 4. Boundary identification markers for single sand bodies.

In the study area, the underwater distributary channel microfacies are well developed. Individual channel sand bodies overlap and cut into each other, forming extensive, continuous thick composite channel sand bodies. Based on the analysis of sedimentary microfacies in each single layer, correlation profiles perpendicular to the sediment source direction

were established. Using the five markers for identifying the boundaries of individual channel sand bodies, the boundaries were recognized on the well-to-well profiles. The boundary points were then marked on a planar map to trace the channel flow direction and extent. Profiles parallel to the sediment source direction were used to determine the channel extension distance. Finally, the boundary points were reasonably connected on the planar map to create a distribution map of individual channel sand bodies [35].

Taking the Chang 8_2^{2-2-1} layer as an example, a hierarchical analysis was conducted from composite channels to individual channels. Figure 5 illustrates the planar distribution of sedimentary microfacies in the Chang 8_2^{2-2-1} layer, where the composite channel sand bodies display a continuous distribution pattern. By creating horizontal and vertical profiles and applying the five identification markers, channel boundaries were identified.
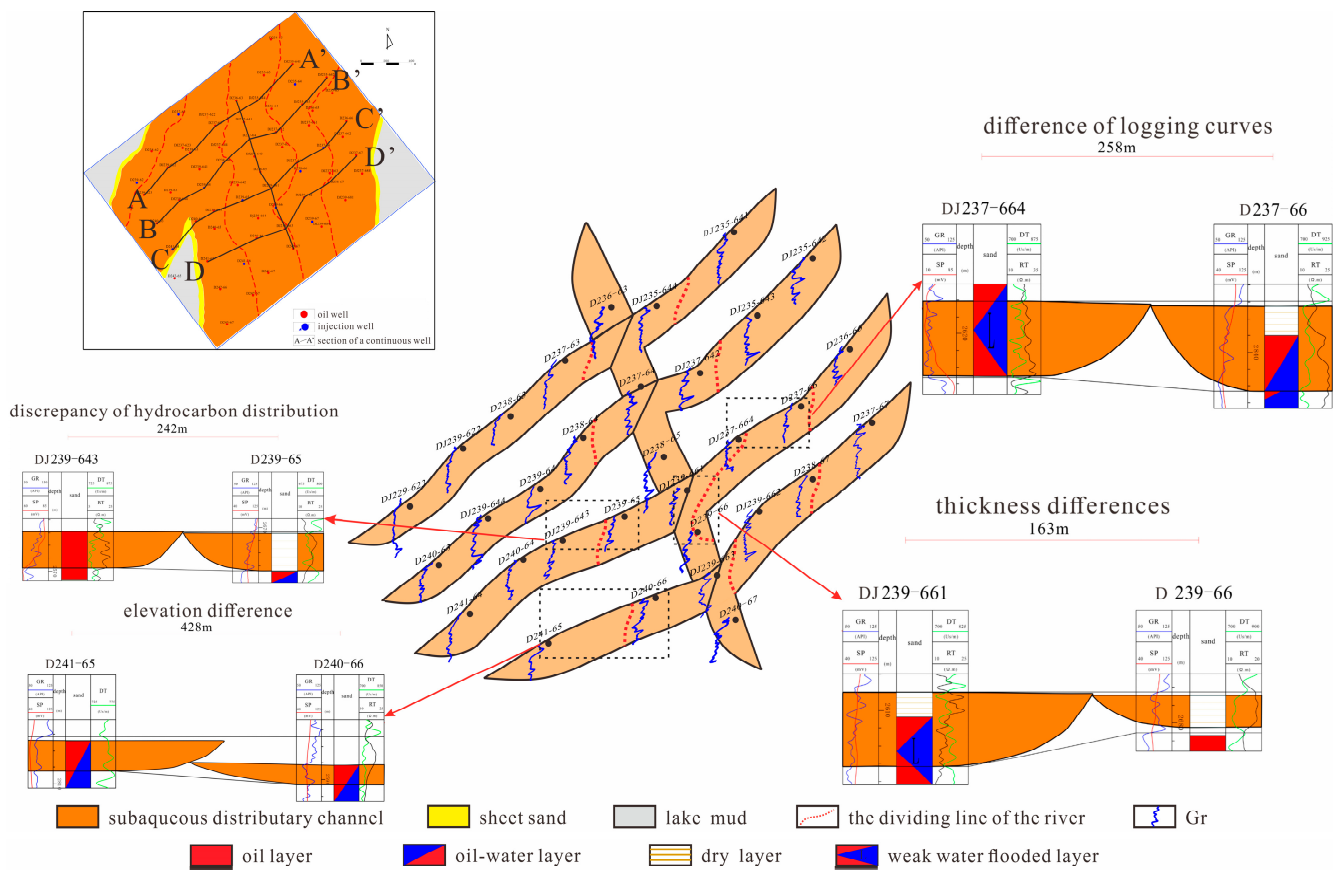

Figure 5. Architecture analysis results of the Chang 8_2^{2-2-1}.

In the CC' profile, well DJ239-643 is interpreted as an oil layer, while D239-65 is a dry layer. Based on the difference in oil and gas content, a channel boundary is identified in this location. Additionally, in well DJ237-664, the natural gamma curve is box-shaped, whereas in D237-66, it is bell-shaped. The difference in logging curve morphology also indicates a channel boundary here.

In the DD' profile, the thickness difference between wells D241-65 and D240-66 is minimal, and both wells contain oil–water transition zones. However, the top elevation of D241-65 is significantly higher than D240-66, suggesting a boundary between the two wells. In the vertical profile, wells DJ239-661 and D239-66 are divided into two distinct channels due to thickness differences.

Using the above tracking methods, the layer was ultimately subdivided into five individual channels (Figure 5). Among these, the second channel from west to east is the largest, with a width exceeding 500 m and an average thickness of 6.1 m. The westernmost

channel is the smallest, with a width of approximately 181 m and a maximum thickness of 9.5 m. The five channels exhibit lateral stacking and overlapping relationships, with only the second channel bifurcating at the lower part, separated by mudstone.

3.2.2. Sand Body Architectural Styles

Sand body architectural patterns are a part of reservoir architecture. By analyzing the patterns and characteristics of sand body architecture, the connectivity between sand bodies can be evaluated, providing constructive insights for the exploration of remaining oil in later stages [36–40].

Combination Styles

Individual sand bodies interact and combine to form composite sand bodies. In the study area, the combination styles of single sand bodies include lateral amalgamation and vertical stacking [33].

(1)   Lateral Amalgamation

During deltaic sedimentation, multiple subaqueous distributary channels transport sediment to the basin in different locations within the same period. These distributary channels advance, forming widespread sheet sands. As a result, multiple underwater distributary channel sand bodies or sheet sand bodies laterally amalgamate within the same single layer [41–45]. Based on the architectural analysis results, four types of lateral amalgamation patterns for single sand bodies were identified in the study area (Table 1).

a.   Underwater Distributary Channel–Underwater Distributary Channel Lateral Amalgamation: In the shallow-water delta front, limited accommodation space causes adjacent distributary channels to laterally migrate and amalgamate, forming contiguous sand bodies. This pattern is characterized by contact along channel edges, where channel boundaries intersect. Channel elevations are generally consistent, and erosion is minimal.

b.   Underwater Distributary Channel–Sheet Sand Lateral Amalgamation: Sand material transported and modified by lake waves and distributary channels forms sheet sands on the channel flanks or in front of the channels. These sheet sands amalgamate with distributary channels to form continuous sand bodies. The boundaries between the two are often difficult to distinguish.

c.   Underwater Distributary Channel–Underwater Distributary Channel Lateral Cutting and Overlapping: During lateral migration, one channel erodes and cuts into an adjacent channel, or a later-stage channel incises into a previously deposited channel. This results in a lateral contiguous but vertically overlapping pattern.

d.   Underwater Distributary Channel Separated by Mudstone: When sediment supply is insufficient, underwater distributary channel sand bodies are laterally separated by mudstone, resulting in non-connected sand bodies.
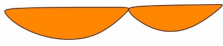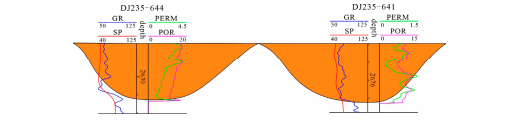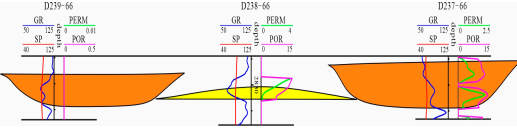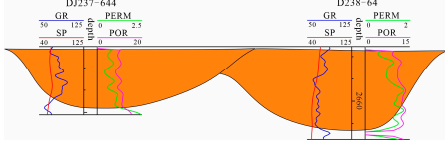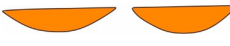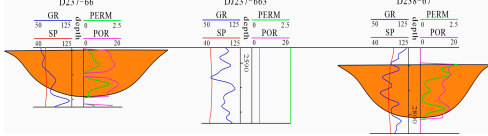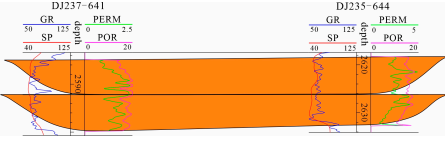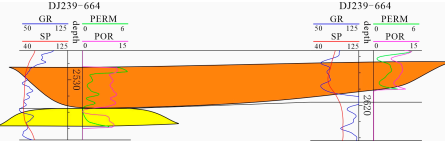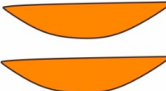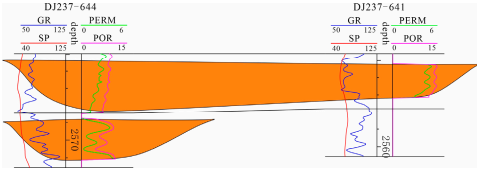
(2)   Vertical Stacking

Wu et al. [33] analyzed the vertical stacking patterns of sand bodies within a short-term cyclic sedimentary period and concluded that the stacking patterns are primarily composite and isolated. Within the same sand group or layer, vertical stacking styles of subaqueous distributary channel and sheet sands are influenced by channel incision and lake-level fluctuations. In the study area, three main vertical stacking styles were identified (Table 1).

a.   Underwater Distributary Channel–Underwater Distributary Channel Stacking: In environments with sufficient sediment supply and strong hydrodynamic forces, the incision of subaqueous distributary channels is significant. Later-stage channels

cut into previously deposited channel sediments, forming vertically thick stacked sand bodies.

b. Underwater Distributary Channel–Sheet Sand Stacking: Similar to the channel–channel stacking type, later-stage channels stack on top of previously deposited sheet sands. As sediment transport advances downstream along the sediment source direction, hydrodynamic energy decreases, reducing the channel incision capability. This prevents complete erosion of the sheet sands, resulting in a combination that forms thick sand bodies.

c. Underwater Distributary Channel–Underwater Distributary Channel Vertical Separation: In the shallow-water delta front, channel sand bodies are separated vertically by thick lacustrine mudstones or thin mudstone interlayers within distributary channel accretion bodies. These separations cause flow barriers within the same sand body, leading to disconnected upper and lower sand bodies.

Table 1. Single sand body combination styles in the study area.

Single Sand Body Combination Style		Combined Model	Example of the Study Area
lateral splicing	Underwater distributary channel–underwater distributary channel lateral splicing type		
	Underwater distributary channel–sheet sand lateral splicing type		
lateral cut stacking	Underwater distributary channel–underwater distributary channel lateral cut stack type		
lateral separation	Underwater distributary channel separated by mudstone type		
vertical superposition	Underwater distributary channel–underwater distributary channel superimposed type		
	Underwater distributary channel–sheet sand superimposed type		
vertical isolation	Underwater distributary channel–underwater distributary channel vertical separation type		

As subaqueous distributary channels develop downstream, the types, sizes, and stacking patterns of channel sand bodies exhibit certain correlations. Statistical analysis (Figure 6) shows that the primary reservoir layers in the study area are dominated by

lateral amalgamation patterns, accounting for approximately 77.15% of cases, while vertical stacking types are the main feature in vertical sections, comprising 74.63% of cases. In contrast, non-primary reservoir layers are dominated by lateral separation and vertical isolation patterns.
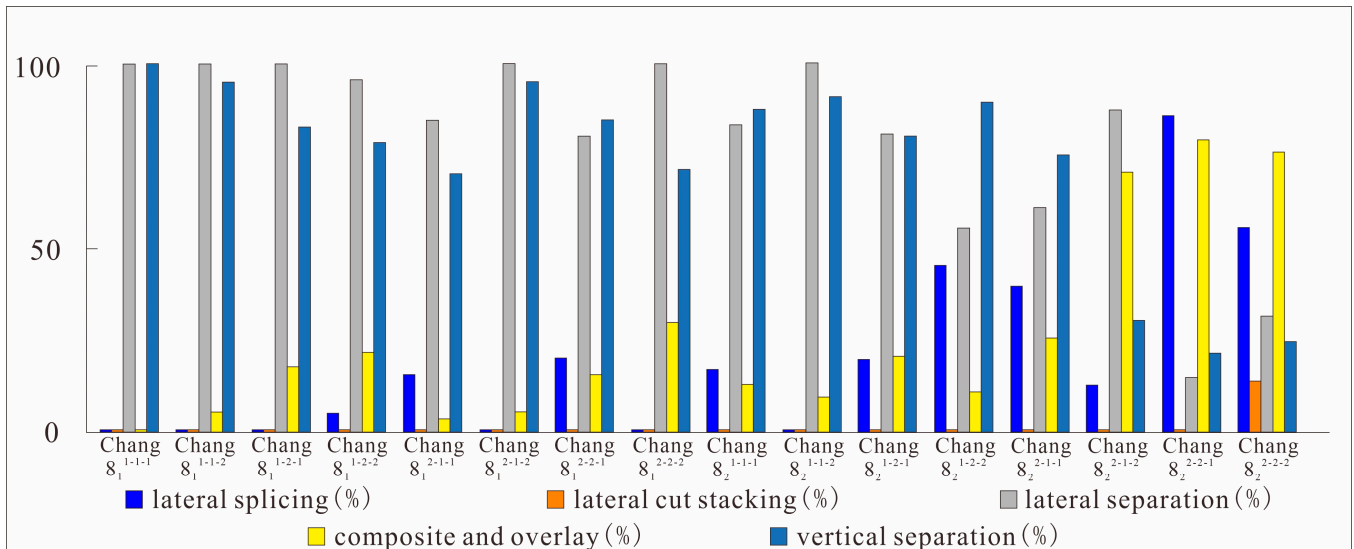
Figure 6. Statistics of architectural contact relationships.

Quantitative Dimensions of Sand Bodies

Based on the results of individual sand body analysis, the quantitative dimensions of single subaqueous distributary channels in the study area were evaluated, and a correlation between thickness and width was established. The single underwater distributary channel sand bodies exhibit relatively large development scales, with thicknesses ranging from 1.31 to 9.00 m and widths ranging from 83.00 to 723.00 m. The distribution is primarily concentrated within the 100.00–200.00 m range. The average width-to-thickness ratio is approximately 52:1 (Figure 7a). A logarithmic correlation between sand body width and thickness was observed, with an overall good fit and a correlation coefficient of approximately 0.74 (Figure 7b).

(a)cumulative frequency distribution of channel sand body width

Figure 7. *Cont.*

(b)relationship between thickness and width of channel sand body

Figure 7. Statistical analysis of single underwater distributary channel sand body dimensions.

4. Results

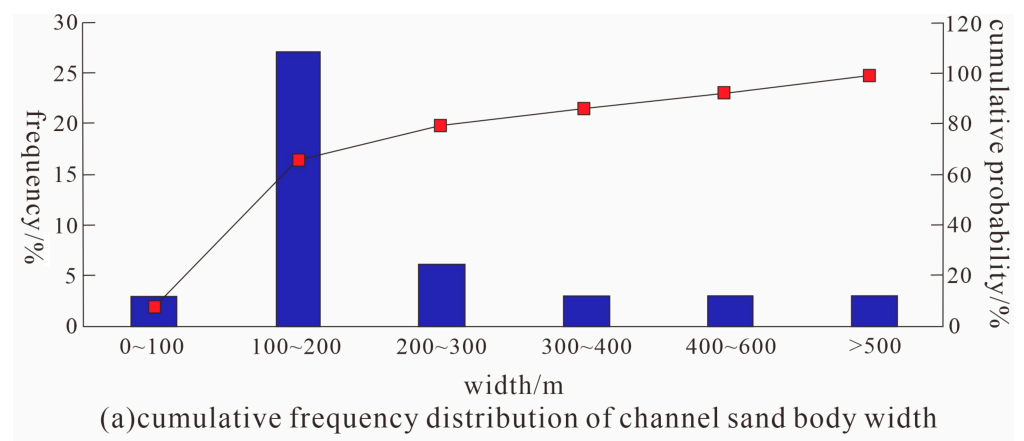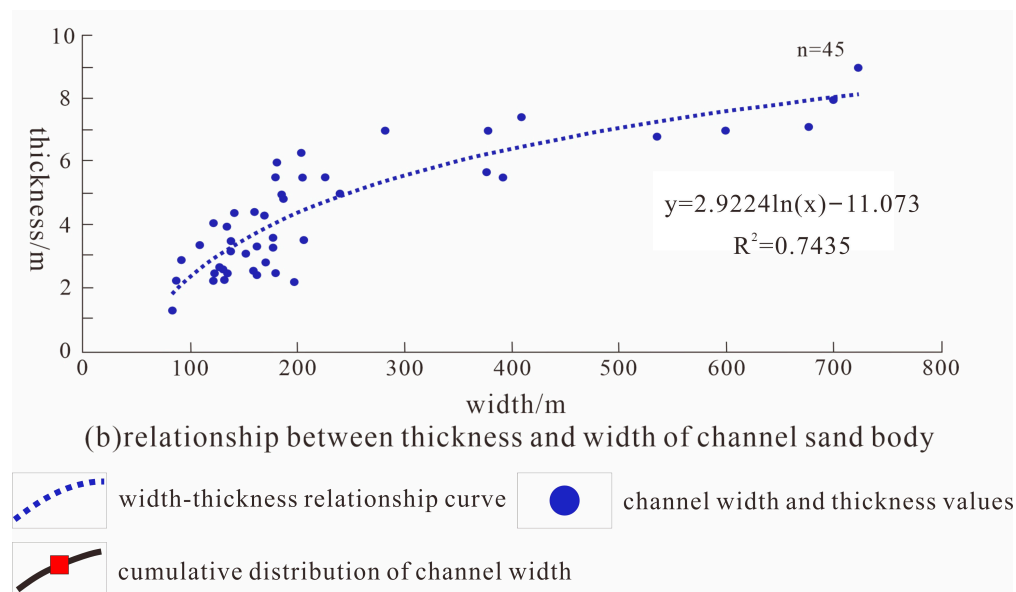To validate the results of reservoir architectural analysis and better guide the later stages of oilfield development, a comprehensive evaluation was conducted. This included analyzing perforation intervals layer by layer, assessing the effectiveness of tracer injections, and examining oil and water production curves for injection–production correspondence. These findings were further corroborated by integrating cross-sectional facies maps to verify the accuracy of sand body architectural interpretations [46–50].

Taking the single-layer well group of Chang $8_2^{2\text{-}2\text{-}1}$ in the study area, represented by well D238-64 (Figure 8), as an example, D238-64 is a tracer injection well. The monitoring wells associated with this group are D238-65, D238-63, DJ237-643, DJ237-644, DJ239-641, and DJ239-642, with respective distances from D238-64 of 303 m, 274 m, 253 m, 129 m, 194 m, and 208 m. Tracer injection commenced on 29 June 2019, using SZJ-2 as the tracer, with a total injection quantity of 5.0 kg.

The tracer monitoring results indicate that out of the six monitoring wells in the D238-64 well group, two detected the tracer. This confirms that there is a connectivity relationship within the single sand body between the tracer injection well and the monitoring wells in this layer. From the tracer production concentration curve (Figure 8c), the single and sharp peak suggests significant vertical heterogeneity within the reservoir of the well group. The injection well and the two tracer-detected wells are located within the same channel unit.

In terms of well spacing, the monitoring wells closer to the injection well detected the tracer earlier, while those farther away may have been blocked by flow barriers within the reservoir. Regarding tracer detection direction, well DJ237-644 detected the tracer earlier than DJ239-641, with the former having higher permeability than the latter. This indicates that medium- to high-permeability zones serve as the primary pathways for tracer migration. Well D238-63, although within the same channel as the injection well, did not detect the tracer because it was not perforated in this layer [51–56].

In Figure 8d, the injection volume for well D238-64 began to increase in October 2019. Correspondingly, the daily liquid production and water cut for well D239-641 also increased. Subsequently, as the injection volume decreased, the water cut also declined in May 2020, demonstrating a strong response and confirming that the two wells belong to the same channel. Wells DJ239-641, DJ237-644, and D238-64 are all classified as poor oil

layers or oil layers, with natural gamma curves showing a box shape, placing them in the same channel. However, wells D237-643 and D239-642, classified as weakly water-flooded layers, are not effectively connected to the injection well D238-64 due to differences in oil and gas characteristics (Figure 8f), indicating they belong to different channels with poor connectivity. This architectural interpretation aligns well with the tracer detection results and production curves, thereby validating the accuracy of the architectural analysis.
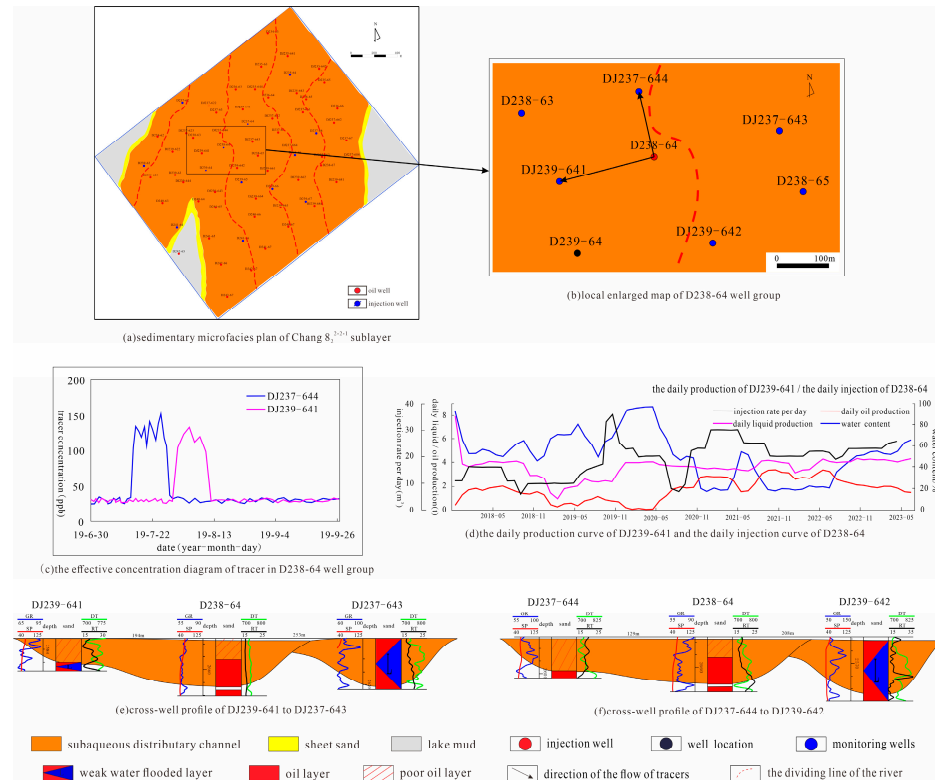

Figure 8. Dynamic verification analysis diagram of D238-64 well group.

According to the statistics, the study area contains 22 water injection wells corresponding to 58 production wells. Among them, 21 wells are effective, and 13 wells have been converted to injection wells. Within single distributary channels, injection–production connectivity is good, whereas connectivity between different distributary channels is poor, with only 25.97% of channels being connected (Table 2). This indicates that the development of ultra-low-permeability reservoirs is primarily controlled by the scale of individual distributary channels. These findings provide a reference for the exploration of remaining oil and the optimization of development strategies in the Luo 1 well area.

Table 2. Injection–production correspondence in the study area.

| Layer | Injection and Production | | Injection–Production Does Not Correspond to the Situation | | | | | |
| | | | Injection Without Production | | No Injection with Production | | No Injection Without Production | |
	Well Numbers	Proportion (%)	Well Numbers	Proportion (%)	Well Numbers	Proportion (%)	Well Numbers	Proportion (%)
Chang$8_1^{2\text{-}1\text{-}2}$	3	4.4	0	0	3	4.4	62	91.2
Chang$8_2^{2\text{-}2\text{-}1}$	29	42.6	0	0	18	26.5	21	30.9
Chang$8_2^{2\text{-}2\text{-}2}$	21	30.9	0	0	15	22.1	32	47

5. Discussion

This study reveals the complex sedimentary architecture of the Chang 8 oil group in the Luo 1 well area of the Jiyuan Oilfield, which has important implications for oil reservoir

development. The reservoir, characterized by ultra-low permeability (0.84 mD), highlights the need to understand the internal architecture of sand bodies and their heterogeneity for optimizing extraction methods. The study's findings on ultra-low-permeability reservoir architecture provide a critical foundation for optimizing oil recovery strategies. By enhancing our understanding of sand body distribution and connectivity, this research can significantly improve reservoir management practices in China and other Asian countries facing similar geological challenges. Tailored development plans based on these insights can lead to more efficient exploitation of remaining oil resources, thereby contributing to regional energy security.

From a socio-environmental standpoint, the enhanced recovery efficiency proposed by this study could reduce the environmental footprint of oil extraction by maximizing production from existing wells. This innovation not only offers economic benefits but also aligns with sustainability goals. Chinese environmental agencies have increasingly emphasized green development, and this research supports that agenda by promoting more sustainable resource utilization methods.

To strengthen the validation of our results, we compare them with previous studies on deltaic depositional systems. Unlike earlier works that often lacked detailed architectural configuration analysis, our study provides new insights into the scale of distributary channels, which are crucial for effective reservoir development. This comparative approach underscores the novelty and value-added contributions of our findings [55,56].

The depositional environment of the study area, a shallow-water delta, is confirmed by the identification of three major sedimentary microfacies: subaqueous distributary channel, finger sand dam, and lake mud. These microfacies, particularly the subaqueous distributary channels, dominate the reservoir architecture. The formation of composite channel sand bodies through lateral splicing and stacking of 2–5 single channels plays a crucial role in storage capacity. The large width of these sand bodies (over 2000 m) suggests a highly interconnected sedimentary system, but their vertical and lateral heterogeneity presents challenges for development, particularly in an ultra-low-permeability context.

Our study also reveals that connectivity between individual distributary channels is poor, with only 25.97% of the channels connected. This low connectivity underscores the importance of focusing on individual channel fills, where injection and extraction processes are better aligned. These findings indicate that the development of ultra-low-permeability reservoirs in this region is largely controlled by the scale and continuity of individual distributary channels.

A key insight from this study is that understanding the sand body architecture, particularly foresets and foreset sand bodies, is essential for improving enhanced oil recovery methods, such as acid fracturing. The correlation between the internal structure of distributary channels and remaining oil distribution suggests that future development should focus on optimizing injection strategies tailored to the sand body architecture.

However, this study has certain limitations. Due to the reliance on limited well data and logging information, the sample size is relatively small, which may not fully reflect the reservoir characteristics of the entire oilfield. Additionally, the heterogeneity of the reservoir is more complex in practice, and future research should integrate a broader range of geological data and numerical modeling to improve the accuracy and general applicability of the conclusions.

6. Conclusions

This study identified the delta-front subfacies in the research area based on previous findings, outcrop sand body characteristics, and well logging responses. Three microfacies were recognized: subaqueous distributary channels, sheet sands, and lacustrine mud.

Notably, subaqueous distributary channels are relatively small in scale, typically less than 300 m wide and spanning no more than two well spacings.

To delineate delta-front reservoir architectural boundaries, we adopted a "vertical phasing and lateral boundary delineation" approach. Five types of markers were established, enabling detailed tracking of profiles and the identification of single architectural sand body boundaries. This method facilitated a comprehensive architectural analysis of contiguous single sand bodies within the study area. Two major architectural patterns—isolated and stacked—were summarized for the study area, further subdivided into seven stacking styles.

In primary reservoir layers, lateral amalgamation patterns dominate (77.15%), while vertical stacking patterns are most common in vertical sections (74.63%). Non-primary reservoir layers, however, are primarily characterized by lateral isolation and vertical separation. These findings indicate that ultra-low-permeability reservoir development is mainly controlled by the scale of individual distributary channels.

While this study provides valuable insights, several challenges remain: The scale and complexity of subaqueous distributary channels require higher-resolution data for more accurate characterization. Further research should focus on integrating seismic data with well logs to enhance the understanding of reservoir architecture at larger scales. Investigating the impact of sediment supply and paleogeography on the distribution and connectivity of sand bodies could provide additional context for reservoir management strategies.

Future work should aim to refine the architectural models through multi-disciplinary approaches, incorporating advanced geophysical techniques and numerical simulations. Addressing these limitations will contribute to more effective reservoir exploitation and management practices.

Author Contributions: Conceptualization, J.W.; methodology, L.W.; software, Y.Y.; validation, P.X. and G.X.; writing—original draft preparation, J.W.; writing—review and editing, L.W.; supervision, P.X.; project administration, Y.Y.; funding acquisition, Y.Y. All authors have read and agreed to the published version of the manuscript.

Institutional Review Board Statement: Not applicable.

Informed Consent Statement: Not applicable.

Data Availability Statement: The data presented in this study are available on request from the corresponding author. The data are not publicly available due to ongoing research using a part of the data.

Conflicts of Interest: The authors declare no conflicts of interest.

References

1. Fisk, H.N.; Mcfarlan, E.J.; Kolb, C.R.; Wilbert, L.J., Jr. Sedimentary framework of the modern Mississippi delta. *J. Sediment. Petrol.* **1954**, *24*, 76–79. [CrossRef]
2. Donaldon, A.C. Pennsylvanian sedimention of Central Appala-chians. *Geol. Soc. Am. Spec. Pap.* **1974**, *148*, 47–48.
3. Yuan, L.; Hu, M.; Deng, Q. Sedimentary Evolution Laws and Main Controlling Factors of the Nenjiang Formation in the Songnan Da'anbei Area, China. *Appl. Sci.* **2024**, *14*, 5269. [CrossRef]
4. Zhao, G.; Zhu, R.; Si, Z.; Liu, M. The Association Between Sand Body Distribution and Fault of Zhuhai Formation on the North Slope of Baiyun Sag, Pearl River Mouth Basin, China. *Appl. Sci.* **2025**, *15*, 412. [CrossRef]
5. Nichols, G.; Fisher, J. Processes, facies and architecture of fluvial distributary system deposits. *Sediment. Geol.* **2007**, *195*, 75–90, ISSN 0037-0738. [CrossRef]
6. Miall, A.D. A review of the braided-river depositional environment. *Earth-Sci. Rev.* **1977**, *13*, 1–62. [CrossRef]
7. Xu, Z.; Wu, S.; Liu, Z. Sandbody architecture of the bar finger within shoal water delta front: Insights from the Lower Member of Minghuazhen Formation, Neogene, Bohai BZ25 Oilfield, Bohai Bay Basin, East China. *Pet. Explor. Dev.* **2019**, *46*, 322–333. [CrossRef]

8.   Yang, T.; Liang, Y.; Wang, Z.; Ji, Q. Dynamic Prediction of Shale Gas Drilling Costs Based on Machine Learning. *Appl. Sci.* **2024**, *14*, 10984. [CrossRef]

9.   Su, S.; Hu, M.; Deng, Q. Relationship between source difference and spatial distribution of sand bodies of shallow—Water delta: An instance of Putaohua Oil Layer in the Western Changyuan, Songliao Basin. *J. Northeast Pet. Univ.* **2021**, *45*, 32–44+7.

10. Zhu, X.; Deng, X.; Liu, Z. Sedimentary characteristics and model of shallow braided delta in large-scale lacustrine: An example from Triassic Yanchang Formation in Ordos Basin. *Geosci. Front.* **2013**, *20*, 19–28.

11. Wu, F.; Li, W.; Li, Y. Delta sediments and evolution of the Yanchang Formation of Upper Triassic in Ordos Basin. *J. Palaeogeogr.* **2004**, *6*, 307–315.

12. Wang, C.; Zheng, R.; Li, Z. Characteristics of Lithologic Reservoir of Interval 8 of Yanchang Formation in Jiyuan Oilfield of Ordos Basin. *Geol. Sci. Technol. Inf.* **2010**, *29*, 69–74.

13. Li, Y.; Liu, C.; Du, Y. Sedimentary characteristics of shallow water delta and lake shoreline control on sandbodies of Chang 8 oil bearing interval of the Upper Triassic Yanchang Formation in northwestern Ordos Basin. *J. Palaeogeogr.* **2009**, *11*, 265–274.

14. Wang, K.; Zhao, J.; Xue, R. Fluvial Sedimentary Types and Their Evolution in the Yan'an Formation in the Ordos Basin: Evidence from the detailed anatomy of typical outcrops. *Acta Sedimentol. Sin.* **2022**, *40*, 1367–1377.

15. Yang, H.; Dou, W.; Liu, X. Analysis on Sedimentary Facies of Member 7 in Yanchang Formation of Triassic in Ordos Basin. *Acta Sedimentol. Sin.* **2010**, *28*, 254–263.

16. Zhang, Y.; Hou, L.; Cui, J. Evolution characteristics of thermal expansion coefficient of rocks with temperature of Triassic Chang 7 organic-rich reservoir and its implications in Ordos Basin. *Lithol. Reserv.* **2022**, *34*, 32–41.

17. Zhu, Y.; Zhao, Z.; Zhang, D. Accumulation conditions and accumulation laws of tight gas in Shenfu area, northeast of Ordos Basin. *China Offshore Oil Gas* **2022**, *34*, 55–64.

18. Deng, X.; Fu, J.; Yao, J. Sedimentary facies of the Middle-Upper Triassic Yanchang formation in Ordos basin and breakthrough in petroleum exploration. *J. Palaeogeogr.* **2011**, *13*, 443–455.

19. Ren, Y.; Zhao, J.; Chen, J. Sedimentary Characteristics and Sand Body Architecture of Shallow Delta Front in Ordos Basin: A Case Study of Chang 9 Member in Shiwanghe Section in Yichuan. *Xinjiang Pet. Geol.* **2022**, *43*, 310–319.

20. Lu, W.; An, X.; Liu, Y.; Li, D.; Zeng, L.; Huangpu, Z.; Tang, Y.; Zhang, K.; Zhang, Y. Dynamic responses and evolutionary characteristics of waterflood-induced fractures in tight sandstone reservoirs: A case study of oil reservoirs in the 8th member of the Yanchang Formation, well block L, Jiyuan oilfield, Ordos Basin. *Oil Gas Geol.* **2024**, *45*, 1431–1446. [CrossRef]

21. Yang, Y.; Ma, Y. Recognition and Application of Single Sand Body Characterization in the Jiyuan Oilfield. *Tianjin Chem. Ind.* **2024**, *38*, 52–55.

22. Zhang, W.; Zhang, X.; Zou, Y.; Wu, Q. Study on Distribution Pattern and Effective Utilization of Remaining Oil in High Water Cut Stage in JIYUAN Oilfield. *Inner Mong. Pet. Chem.* **2024**, *50*, 101–105.

23. Meng, Q.; Cheng, Y.; Teng, F.; Li, J.; Wu, G.; Zhao, L. Reservoir Architecture and Residual Oil Distribution Characteristics of Distal Submarine Fans: A Case Study of the NS Fault Block in the Huanghua Sag. *N. China Geol.* **2024**, *47*, 66–76.

24. Li, W.; Liu, Y.; Gao, T. Characterization of single sandbody in the subphase background of shallow water delta front: Taking Chang4+5 reservoir in YGS block of Dingbian Oilfield as an example. *Unconv. Oil Gas* **2023**, *10*, 65–74.

25. Zhang, F.; Ma, X.; Dong, Z.; Zou, L.; Wang, X.; Li, W.; Wu, L. Application of Machine Learning Models Based on CNN and LSTM in Logging Lithology Identification. *J. Xi'an Univ. Pet. (Nat. Sci. Ed.)* **2024**, *39*, 96–103, 133.

26. Zhang, Z.; Liu, L. Lithology Classification Using Machine Learning Algorithms Based on SDGSAT-1 TIS. *Geol. Rev.* **2024**, *70* (Suppl. S1), 351–352.

27. Zhang, Q.; Wang, L.; Liu, L.; Wang, Y. Study on Lithology Classification Method Based on Lithology Index and Three-Dimensional Feature Space. *Acta Geol. Sin.* **2025**, 1–12. [CrossRef]

28. Cheng, G.; Zhou, D.; Li, G.; Wang, Y.; Peng, L. Sedimentary Characteristics and Favorable Reservoir Prediction of the Second Member of the Triassic Baijiantan Formation in Mahu 1 Well Area. *Spec. Oil Gas. Reserv.* **2024**, *31*, 49–56+66.

29. Ren, Y.; Yan, J.; Wang, M.; Song, D.; Geng, B. Grain Size Logging Inversion Method for Complex Clastic Rocks and Its Application in Detailed Lithology Identification. *J. Palaeogeogr.* **2024**, 1–16.

30. Liu, S.; Yu, Z.; Gao, Q.; Ba, S.; Jin, C.; Luo, L. Interbed detection and oil-gas characteristics in shale oil reservoir in bonan depression base on well logging curve reprocessing. *Geophys. Geochem. Explor.* **2024**, *46*, 26–34.

31. Zhang, W.; Wang, T.; Shao, D.; Zhu, J.; He, J.; Lei, Y.; Gao, X.; He, C.; Song, H.; Hu, Y. Distribution and Potential Evaluation of the Chang 9 Source Rock in the Longdong Area of the Ordos Basin. *Nat. Gas. Geosci.* **2024**, *35*, 465–478.

32. Kang, Q.; Gao, Z.; Liu, C.; Yang, M.; Zhang, D. Depositional Microfacies Types and Distribution Characteristics of the Chang 6 Oil Layer in the Wangjiagou Area. *Yunnan Chem. Ind.* **2021**, *48*, 123–125.

33. Ma, L.; Song, B.; Yu, C. Single sandbody architecture characteristics of fan-delta front reservoir in a small lacustrine rift basin: A case study of the Es31 oil formation, Gao 76 fault block, Nanpu Sag. *J. Northeast Pet. Univ.* **2023**, *47*, 1–17.

34. Yin, Y.; Ding, W.; An, X. Configuration characterization of Triassic Chang 611reservoir in Sai 160 well area of Ansai oilfield, Ordos Basin. *Lithol. Reserv.* **2023**, *35*, 37–49.

35. Zhao, J.; Wang, H.; Zhang, D.; Sun, H.; Chen, G.; Yin, S. Advances in the Study of Depositional Architecture and Characterization of Marine Sandy Shoreface Deposits. *Acta Sedimentol. Sin.* **2025**, 1–23. [CrossRef]

36. Zhao, X.; Bao, Z.; Liu, Z. An in-depth analysis of reservoir architecture of underwater distributary channel sand bodies in a river dominated delta: A case study of T51 Block, Fuyu Oilfield. *Pet. Explor. Dev.* **2013**, *40*, 181–187. [CrossRef]

37. Liang, X.; Xian, B.; Feng, S. Architecture and Main Controls of Gravity-flow Sandbodies in Chang 7 Member, Longdong Area, Ordos Basin. *Acta Sedimentol. Sin.* **2022**, *40*, 641–652.

38. Wu, S.; Xu, Z.; Liu, Z. Depositional architecture of fluvial-dominated shoal water delta. *J. Palaeogeogr.* **2019**, *21*, 202–215.

39. Ren, S.; Yao, G.; Mao, W. Genetic Types and Superimposition Patterns of Subaqueous Distributary Channel Thin Sandbodies in Delta Front: A case study from the IV–VI reservoir groups of H3 in Biqian 10 area of Gucheng oilfield. *Acta Sedimentol. Sin.* **2016**, *34*, 582–593.

40. Zhang, L.; Bao, Z.; Lin, Y. Genetic types and sedimentary model of sandbodies in a shallow-water delta: A case study of the first Member of Cretaceous Yaojia Formation in Qian'an area, south of Songliao Basin, NE China. *Pet. Explor. Dev.* **2017**, *44*, 727–736. [CrossRef]

41. Wu, S.; Yue, D.; Feng, W. Research progress of deposition architecture of clastic systems. *J. Palaeogeogr.* **2021**, *23*, 245–262.

42. Jia, C.; Xiao, M.; Li, M.; Tai, C.; Yang, W.; Gao, H.; Meng, R. Application of modeling method of meandering river point bar architecture in Gangdong Oilfield. *Complex Oil Gas Reserv.* **2023**, *16*, 301–307.

43. Budai, S.; Colombera, L.; Mountney, N.P. Quantitative characterization of the sedimentary architecture of Gilbert-type deltas. *Sediment. Geol.* **2021**, *426*, 106022, ISSN 0037-0738.

44. Miall, A.D. Architectural-element analysis: A new method of facies analysis applied to fluvial deposits. *Earth-Sci. Rev.* **1985**, *22*, 261–308. [CrossRef]

45. Steel, R.; Osman, A.; Rossi, V.M.; Alabdullatif, J.; Olariu, C.; Peng, Y.; Rey, F. Subaqueous deltas in the stratigraphic record: Catching up with the marine geologists. *Earth-Sci. Rev.* **2024**, *256*, 104879, ISSN 0012-8252. [CrossRef]

46. Jorissen, E.L.; de Leeuw, A.; van Baak, C.G.; Mandic, O.; Stoica, M.; Abels, H.A.; Krijgsman, W. Sedimentary architecture and depositional controls of a Pliocene river-dominated delta in the semi-isolated Dacian Basin, Black Sea. *Sediment. Geol.* **2018**, *368*, 1–23, ISSN 0037-0738. [CrossRef]

47. Rossi, V.M.; Kim, W.; Leva López, J.; Edmonds, D.; Geleynse, N.; Olariu, C.; Steel, R.J.; Hiatt, M.; Passalacqua, P. Impact of tidal currents on delta-channel deepening, stratigraphic architecture, and sediment bypass beyond the shoreline. *Geology* **2016**, *44*, 927–930. [CrossRef]

48. Tian, B.; Duan, Z.; Zhao, J.; Zheng, Y. Detailed architecture analyses of sandy braided bar reservoir: A case study of Sulige Gas Filed. *Unconv. Oil Gas* **2023**, *10*, 9–17.

49. Eilertsen, R.S.; Corner, G.D.; Aasheim, O.; Hansen, L. Facies characteristics and architecture related to palaeodepth of Holocene fjord–delta sediments. *Sedimentology* **2011**, *58*, 1784–1809. [CrossRef]

50. Hori, K.; Saito, Y.; Zhao, Q.; Wang, P. Architecture and evolution of the tide-dominated Changjiang (Yangtze) River delta, China. *Sediment. Geol.* **2002**, *146*, 249–264. [CrossRef]

51. Martini, I.; Ambrosetti, E.; Sandrelli, F. The role of sediment supply in large-scale stratigraphic architecture of ancient Gilbert-type deltas (Pliocene Siena-Radicofani Basin, Italy). *Sediment. Geol.* **2017**, *350*, 23–41.

52. Deptuck, M.E.; Steffens, G.S.; Barton, M.; Pirmez, C. Architecture and evolution of upper fan channel-belts on the Niger Delta slope and in the Arabian Sea. *Mar. Pet. Geol.* **2003**, *20*, 649–676.

53. Hicks, N.; Green, A. Sedimentology and depositional architecture of a submarine delta-fan complex in the Durban Basin, South Africa. *Mar. Pet. Geol.* **2016**, *78*, 390–404. [CrossRef]

54. Rohais, S.; Eschard, R.; Guillocheau, F. Depositional model and stratigraphic architecture of rift climax Gilbert-type fan deltas (Gulf of Corinth, Greece). *Sediment. Geol.* **2008**, *210*, 132–145.

55. Guo, J.; Li, J.; Wang, Z.; Gong, D. Architectural Characterization of Braided River Reservoirs in the Southern Area of the Gu Islands Oilfield. *Sci. Technol. Eng.* **2023**, *23*, 8148–8161.

56. Zhao, J.; Sun, H.; Fang, H.; Tian, L.; Zheng, X.; Wang, H. Architecture Patterns and Characterization of Marine Sandy Beach-bar Reservoirs: A case study of the Donghe sandstone in the Hudson oilfield. *Acta Sedimentol. Sin.* **2025**, 1–20. [CrossRef]